Squeezing instabilities and delamination in elastic bilayers: A linear stability analysis

Hemalatha Annepu and Jayati Sarkar*
Department of Chemical Engineering, Indian Institute of Technology Delhi, New Delhi 110 016, India
(Received 27 July 2012; published 9 November 2012)

A linear stability analysis is presented to understand the instabilities that arise in an elastic bilayer, consisting of a very thin bottom layer (thickness < 100 nm) that acts as a *wetting film* and a top layer that acts as an *adhesive film*, when placed in contact proximity with an external rigid contactor. Depending on whichever layer is more compliant, "squeezing modes" of instability with a variety of length scales ranging from $\ll 3h$ to $\gg 3h$ (h: bilayer thickness) are found to be possible. The least length scales obtained are $0.1h$. The squeezing instabilities are, however, accompanied by delamination of the film-film interface. The instability length scales, the strength of interactions required, and the delamination decrease as the compliance of the top film increases. Surface tension effects are found to have a stabilizing influence which increases the instability length scales and decreases the degree of delamination at the cost of high interaction penalty.

DOI: 10.1103/PhysRevE.86.051604 PACS number(s): 68.15.+e, 68.35.Np, 81.16.Rf, 68.65.Ac

I. INTRODUCTION

Instabilities in thin films have been the subject of intensive research activities in the past few decades due to the characteristic patterns they form and their potential for a multitude of applications in flexible electronics [1–3], optoelectronics [4–6], sensors [7,8], pressure sensitive adhesives [9–12], microfluidic devices [13–15], MEMS [16–20], etc. Apart from these technological applications, they are also model mesoscopic systems for understanding physical phenomena such as adhesion-debonding, pattern formation [21–42], wetting-dewetting [43–51], and friction at soft interfaces [52–54]. Single thin films are mainly found in primarily two different configurations: *wetting* and *adhesive*, where in both cases the presence of an external surface induces intermolecular interactions in the film. In *wetting film* the film is cast on a substrate and is generally thin such that the underlying substrate induces van der Waals (VDW) or polar interactions and is able to deform the free film surface. If VDW interactions are present (which is generally the case) the film thickness should be less than 100 nm, to feel such interactions. *Adhesive film*, on the other hand, refers to film of finite thickness cast on a substrate and confined by a contactor. The external contacting surface induces interactions and whenever the film-contactor gap distance is less than a critical value the interactions are strong enough to deform the film surface. Thus, in adhesive film, there is no limit to film thicknesses which can be even semi-infinite. However, the film-contactor gap distances are of importance and are dependent on the nature of interactions present. Substantial work has already been accomplished in wetting liquid thin films (mean film thickness $h < 100$ nm) like polymer melts cast on bare or precoated substrates, where it has been found that they dewet or bead when the destabilizing molecular interactions between the film and the substrate surpass the stabilizing surface tension forces. In these liquid films, the characteristic length scale of instability λ scales nonlinearly with the mean film thickness h ($\lambda \sim h^2$ for van der Waals interactions) and is influenced by both the nature and magnitude of interactions present between the film and the substrate [43–51]. When a soft (shear modulus $\mu < 10$ MPa), thin elastic film of few microns mean film thickness cast on a rigid substrate and confined by van der Waals forces operative due to proximity to an external rigid contactor was used instead, instabilities formed were due to competition between the destabilizing interaction forces between the film and the contactor and the restoring elastic forces present in the bulk of the elastic film. The engendered instabilities in the confined elastic films were of small length scales which scaled linearly with the film thickness as $\sim 3h$. A salient feature of these instabilities is also that they are independent of the nature and magnitude of interactions present between the film and the contactor as well as the surface tension forces [21–42], unlike the liquid films where both the film-substrate interactions and the surface tension play a crucial role in determining the instability length scales.

Much work has been directed since then towards reducing the instability length scales and producing increasingly miniaturized patterns which are useful in several technological applications at micro and nano ranges. Of late, length scales much smaller than $3h$ have been realized with elastic films by methods of using patterned substrates [55] or elastic bilayers [56–59]. Theoretical studies on elastic films bonded to patterned substrates [55] suggested that instabilities with wavelengths up to an order of magnitude smaller than $3h$ can be formed if the substrate can be patterned with high asperity ratios.

Bilayers offer interesting physics because they involve the dynamics of two coupled interfaces, which lead to two initial deformation modes—namely, *bending* or *similar* mode of instability in which both the film-air and film-film interfaces deform completely in-phase, i.e., with a positive amplitude ratio, and *squeezing* or *dissimilar* mode of instability in which the interfaces deform completely out-of-phase such that the amplitude ratio of the deformations at the two interfaces is negative [56–64]. Bilayers can be used to generate a myriad of patterns of different wavelengths of which miniature patterns can also be obtained by tuning the physical parameters that govern the instabilities. In the case of the PDMS-metal bilayer system [60] it was found that the minimum length scales

*jayati@chemical.iitd.ernet.in

obtainable were $\sim 3h$ whereas in viscous-elastic [64] bilayers in confined and free configuration length scales much less than the natural length scales that are observed with either the single elastic film or the viscous film could be attained. In systems of elastic bilayers a similar scenario was observed where smaller length scales, up to even $0.5h$, were achieved [56–59] by tuning the thickness ratios as well as the shear moduli ratios of the two films. The existing theoretical studies on elastic bilayers show that both the film-contactor and the film-film interface always develop *similar* or *bending* modes of instability since they are disturbed by the same interfacial energy at the film-contactor interface. *Squeezing* mode (completely out-of-phase deformations) is energetically highly unfavorable in these bilayer configurations as there are no additional forces operative which oppose this unidirectional pull other than the intrinsic elastic energies of the films, which can at most bring the perfect film-film interface back to being planar but never out-of-phase, as has been confirmed by both linear and nonlinear analysis [57].

A very pertinent question arises: What happens to the instabilities in the elastic bilayers if the bottom layer is now made of a *very thin* film (thickness much less than 100 nm) and forced to act as a *wetting film* (which will trigger interactions with the substrate)? It is well established that when the film is very thin, the interactions of the film with the substrate become important and result in long-wave instabilities [41,43–51]. When the bilayer-contactor gap distance d is less than the critical gap distance d_{crit}, the top surface is attracted to the contactor via VDW interactions and the restoring effect of the elastic films will still lead to short-waved deformation of the film-air interface, typical of thicker soft single adhesive elastic films. The wetting nature of the bottom film, however, will now trigger VDW interactions between the film and the substrate, which will try to attract the film-film interface to the substrate. In case of free elastic wetting films it has been observed that the film dewets from the substrate at large length scales. So it would be interesting to study the predominant length scale of instability in such bilayers and whether the interplay of these antagonistic energies results in squeezing mode of instability. Moreover, in several instances of stiff films cast on compliant elastic substrates it has been found that during indentation tests [65] or during the application of in-plane compressive stresses [66–71], the film undergoes delamination if the film and the substrate are of very dissimilar elastic stiffnesses. It would be intriguing to see, if the stiffnesses of the films are made to be very dissimilar in the elastic bilayer under consideration, whether the squeezing mode of instability can engender delamination at the film-film interface—a phenomena which cannot be established by the concepts of a perfect interface (where there are both stress and displacement continuities) and bending modes of instability as done in the previous studies on elastic bilayers [57]. The present paper utilizes a linear stability formulation to verify whether the squeezing mode of instability is at all energetically favorable and the plausible degree of delamination in such elastic bilayers comprising a very thin bottom layer. It also uncovers the spectrum of wavelengths that are formed and the magnitude of the threshold interaction forces that are required for the inception of such surface instabilities.

II. MATHEMATICAL MODELING

A schematic of the elastic bilayer of lateral length L and total height h is depicted in Fig. 1. The properties of the top and the bottom layers of this initially stress-free bilayer are denoted by superscripts b and a, respectively. Both the films are considered to be soft and hence are considered to have shear moduli values (μ^b and μ^a) less than 10 MPa. The individual thicknesses of the incompressible top and bottom films are h^b and h^a, respectively, and the bottom layer is regarded to have a thickness of magnitude $\ll 100$ nm (the thickness limit of *wetting films*). The bottom layer is thus in a *wetting* configuration; i.e., it is subjected to interactions with the underlying substrate. Both the layers are considered to have the same surface energy γ whose value lies in the range of 0–100 mJ/m^2. The displacement field of the bilayer can be denoted by $\mathbf{u}^m(x_1,x_2)$, where x_1 and x_2 denote the spatial coordinates in the bilayer where the displacement needs to be evaluated. The superscript m is used as a dummy index ($=a$ or b) and indicates the film layer under consideration. The bilayer is present near an external contactor at a gap distance d such that the interaction potential (mainly van der Waals interactions) active between the top surface of the bilayer and the contactor is strong enough to deform the bilayer whenever $d < d_{\text{crit}}$ (critical gap distance).

The van der Waals interaction potential that is effective between the bilayer and the contactor has the following mathematical form:

$$U\left(d - u_2^b(x_1,0)\right) = -\frac{A_h}{12\pi\left[d - u_2^b(x_1,0)\right]^2}, \qquad (1)$$

where d is the air gap and A_h is the Hamaker constant (of the order of 10^{-20} J).

For the linear stability analysis, this potential can be linearized by Taylor expansion about the reference state of the undeformed film and retention of terms up to quadratic order leads to the following form:

$$U\left(u_2^b(x_1,0)\right) = U_0 + F_p u_2^b(x_1,0) + \tfrac{1}{2} Y u_2^b(x_1,0)^2, \qquad (2)$$

where $U_0 = U$, $F_p = (\partial U/\partial u_2^b)$, and $Y = (\partial F_p/\partial u_2^b)$, all calculated at $u_2^b(x_1,0) = 0$.

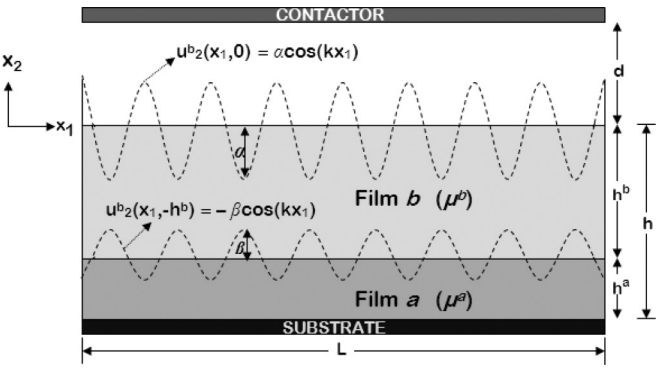

FIG. 1. Schematic diagram of a soft, incompressible elastic bilayer of length L and effective thickness h bonded to a rigid substrate. The film a, directly bonded to the substrate, is of shear modulus μ^a and thickness h^a ($\ll 100$ nm), and the top film b has shear modulus μ^b and thickness h^b.

In the above equation, the term F_p refers to the interaction force per unit area and behaves like a pressure term. Y is the interaction stiffness whose dimensions are that of force per unit volume and it is of importance in determining the conditions for the onset of instability as will be seen later. The contactor, thus, induces a normal traction, of magnitude τ, of the form

$$\tau = -F_p - Yu_2^b(x_1,0) + \gamma u_{2,11}^b(x_1,0). \tag{3}$$

Here the first two terms represent the attractive force (per unit area) that the contactor induces because of intermolecular interactions. The last term denotes the Laplace pressure (associated with weakly curved surfaces) that is present at the curved interface of the elastic bilayer and is a measure of the surface tension forces that need to be overcome in order to deform the top interface. These interactions at the bilayer-contactor interface are counteracted by the elastic stresses in the bulk and the equilibrium stress field that develops in the film due to these antagonistic forces should satisfy the following stress-equilibrium condition:

$$\nabla \cdot \underline{\underline{\sigma}}^m = 0, \tag{4}$$

where, $\underline{\underline{\sigma}}^m = p^m \underline{\underline{\mathbf{I}}} + \mu^m(\nabla \mathbf{u}^m + (\nabla \mathbf{u}^m)^T)$ is the stress field, $\underline{\underline{\mathbf{I}}}$ is the identity tensor, and p^m is the pressure distribution across the film layer m.

In the film interior, the equilibrium displacement also satisfies the incompressibility condition given by

$$\nabla \cdot \mathbf{u}^m = 0. \tag{5}$$

The contactor induces the normal traction at the top surface of the bilayer as given by Eq. (3), and hence at the top interface the film is assumed to be shear free, or

$$\sigma_{12}^b(x_1,0) = 0. \tag{6}$$

The normal traction is considered to result in a sinusoidal surface deformation and the displacement field at the top interface is assumed to take the form

$$u_2^b(x_1,0) = \alpha \cos(kx_1). \tag{7}$$

At the film-substrate interface the displacement field needs to satisfy the rigid boundary condition given by

$$u_2^a(x_1, -h) = 0. \tag{8}$$

It also needs to fulfill the no-slip boundary condition at the film-substrate interface, and hence,

$$u_1^a(x_1, -h) = 0. \tag{9}$$

At the film-film interface the shear stresses are considered continuous. Thus,

$$\sigma_{12}^b(x_1, -h^b) = \sigma_{12}^a(x_1, -h^b). \tag{10}$$

The equality of surface energies of both the layers ensures continuity of normal stresses at the film-film interface which leads to

$$\sigma_{22}^b(x_1, -h^b) = \sigma_{22}^a(x_1, -h^b). \tag{11}$$

The no-slip condition at the film-film interface suggests that the transverse displacements of the two films also need to be the same at this interface. Thus,

$$u_1^b(x_1, -h^b) = u_1^a(x_1, -h^b). \tag{12}$$

The normal traction at the top surface in general is capable of deforming the film-film interface in phase with the top-layer deformation [56–58]. However, in the present study we have considered that the lower film is of very small thickness ($\ll$100 nm). Hence the lower substrate is anticipated to exert a traction at the top interface of the bottom layer via VDW interactions. In addition to the van der Waals interactions, other types of short-range interactions of higher magnitude can also be present (like acid-base interactions [72]) which can also deform the bottom layer. Thus, in the bilayer two types of interactions are considered to be present, one between the top surface of film b and the contactor which can be named as the adhesive interaction [Eq. (1)], which tries to bring the free surface of the bilayer closer to the contactor, and the other between the top surface of film a and the substrate, which can be termed as the wetting interaction and brings the film-film surface closer to the substrate. Possible interactions arising from the interplay of other interfaces, even if they are present, are considered to be of negligible magnitude in comparison to the aforementioned interactions and are neglected in the present study. The film-film interface will thus feel the effect of these two antagonistic interactions and it will be intriguing to see whether the equilibrium displacement field can satisfy a squeezing mode of instability given by

$$u_2^b(x_1, -h^b) = -\beta \cos(kx_1). \tag{13}$$

In the present work the continuity of the transverse displacements given by Eq. (12) ensures a nonslipping and nonsliding interface, a reasonable assumption considering only normal tractions to be present in the bilayer. However, if the films are of very dissimilar stiffnesses there is a possibility that the integrity of the interface may be lost and there may be discontinuity in the normal displacements at the interface under application of normal traction. Such interfaces are different from *perfect* or *welded* interfaces where both stresses and displacements are considered to be continuous. In case of *imperfect interfaces* stresses are considered to be continuous via zones of contact while the displacements can be either continuous or discontinuous and can be accounted for by using a springlike model [73–83] as given below:

$$\begin{aligned}
\sigma_{12}^a(x_1, -h^b) &= \sigma_{12}^b(x_1, -h^b) \\
&= \beta_t\left[u_1^a(x_1,-h^b) - u_1^b(x_1, -h^b)\right], \\
\sigma_{22}^a(x_1, -h^b) &= \sigma_{22}^b(x_1, -h^b) \\
&= \beta_n\left[u_2^a(x_1,-h^b) - u_2^b(x_1, -h^b)\right].
\end{aligned} \tag{14}$$

The parameters β_t and β_n are independent springlike constants or interface imperfection factors and represent the condition of the interface. A completely slipping interface has $\beta_t = 0$. If $\beta_t = \infty$ and $\beta_n = \infty$, it refers to an interface that is perfectly bonded or welded, which is the case considered in the earlier work on elastic bilayers [56,57]. If, on the other hand, $\beta_t = \infty$ and $0 < \beta_n < \infty$, it means the interface is *loose* or *imperfect* and it is precisely the possibility that we are analyzing in the present study. The value of β_n, thus, quantifies the degree of delamination of the film-film interface present, if any, and a very small value of β_n would suggest a large degree of interface delamination.

In general, different wavelengths are possible at the top surface of the film a and the film b and that eliminates clear distinction between bending and squeezing modes. Since such varying wavelengths cannot be handled by the analytics of the linear stability analysis, both films are constrained to deform with similar wavelengths and a clear distinction between bending and squeezing modes is possible and essential. In the absence of prior knowledge of the interface parameters β_n and β_t, the particular condition for the normal displacement at the film-film interface given by Eq. (13) is essential to carry out the linear stability study of elastic bilayers in which the interactions from the substrate too play a crucial role and may deform the film-film interface antagonistic to or out-of-phase from the film-air interface deformations.

In the case of the incompressible films considered, homogeneous deformation leads to zero displacement fields and the uniform pressure field $p^m(x_1,x_2)$ that develops in the films is equal to the parameter $-F_p$ of Eq. (3) [23,41]. If we consider the inhomogeneous displacement and pressure fields that develop in the two layers to be sinusoidal and of the following form:

$$u_1^m(x_1,x_2) = \tilde{u}_1^m(x_2)\sin(kx_1), \quad u_2^m(x_1,x_2) = \tilde{u}_2^m(x_2)\cos(kx_1),$$
$$p^m(x_1,x_2) = \tilde{p}^m(x_2)\cos(kx_1), \tag{15}$$

then the equilibrium conditions to be satisfied [Eqs. (4) and (5)] simplify to

$$\mu^m\left(-k^2\tilde{u}_1^m(x_2) + \frac{d^2\tilde{u}_1^m(x_2)}{dx_2^2}\right) - k\,\tilde{p}^m(x_2) = 0,$$
$$\mu^m\left(-k^2\tilde{u}_2^m(x_2) + \frac{d^2\tilde{u}_2^m(x_2)}{dx_2^2}\right) + \frac{d\,\tilde{p}^m(x_2)}{dx_2} = 0, \tag{16}$$
$$-k\tilde{u}_1^m(x_2) + \frac{d\tilde{u}_2^m(x_2)}{dx_2} = 0.$$

Elimination of the pressure term in the above equations lead to the following biharmonic equation in each film:

$$\frac{d^4\tilde{u}_2^m(x_2)}{dx_2^4} - 2k^2\frac{d^2\tilde{u}_2^m(x_2)}{dx_2^2} + k^4\tilde{u}_2^m(x_2) = 0. \tag{17}$$

The general solution of Eq. (17) for film a yields

$$\tilde{u}_1^a(x_1,x_2) = -\frac{\beta}{k}\{[B + k(A + Bx_2)]e^{kx_2} + [D - k(C + Dx_2)]e^{-kx_2}\}\sin(kx_1),$$
$$\tilde{u}_2^a(x_1,x_2) = \beta[(A + Bx_2)e^{kx_2} + (C + Dx_2)e^{-kx_2}]\cos(kx_1),$$
$$\tilde{p}^a(x_1,x_2) = -2\mu^a\beta(Bx_2e^{kx_2} + Dx_2e^{-kx_2})\cos(kx_1), \tag{18}$$

while that for film b gives

$$\tilde{u}_1^b(x_1,x_2) = -\frac{\alpha}{k}\{[Q + k(P + Qx_2)]e^{kx_2} + [S - k(R + Sx_2)]e^{-kx_2}\}\sin(kx_1),$$
$$\tilde{u}_2^b(x_1,x_2) = \alpha[(P + Qx_2)e^{kx_2} + (R + Sx_2)e^{-kx_2}]\cos(kx_1),$$
$$\tilde{p}^b(x_1,x_2) = -2\mu^b\alpha(Qx_2e^{kx_2} + Sx_2e^{-kx_2})\cos(kx_1). \tag{19}$$

The eight unknowns A,B,C,D,P,Q,R, and S in Eqs. (18) and (19) can be evaluated using the eight boundary conditions of Eqs. (6)–(13) to obtain the specific displacement and pressure fields in the bilayer. If different wave numbers k_1 and k_2 were considered at the film-air and film-film interface, respectively, then Eqs. (15)–(17) and (19) for film b will be in terms of k_1 and Eqs. (15)–(18) for film a will be in terms of k_2. The boundary conditions at the film-film interface involving stress and displacement continuity conditions [given by Eqs. (10)–(12)] will now involve different wave numbers and will not permit cancellation of terms containing sinusoidal variation in x_1. This will prevent further simplification and will result in the unknowns A,B,C,D,P,Q,R, and S in Eqs. (18) and (19) as functions of x_1 in addition to x_2. This contradicts the variable separable assumption of Eq. (15) and the analysis will be incorrect henceforth. Hence, for the linear analysis, we considered both the interfaces to deform at similar length scales as stated earlier.

From the values of the evaluated unknowns, one can evaluate the normal stresses that develop at the surface due to inhomogeneous deformations and pressure field and equate it to the traction that the contactor induces at the top surface via the equation

$$\sigma_{22}^b(x_1,0) = -Yu_2^b(x_1,0) + \gamma u_{2,11}^b(x_1,0). \tag{20}$$

A. Linear stability analysis

To carry forward the analysis, we define here some nondimensional parameters as

$$M = \frac{\mu^a}{\mu^b}, \quad H = \frac{h^b}{h}, \quad q = kh, \quad F = \frac{\beta}{\alpha}. \tag{21}$$

Introduction of these nondimensional parameters in the stress balance equation at the bilayer-air interface [Eq. (20)] leads to the following nondimensional form of the characteristic equation:

$$\frac{-hY}{\mu^b} = S'(M,H,q,F) + q^2\frac{\gamma}{\mu^b h} = S''(M,H,q,F,G). \tag{22}$$

The functional forms of $S''(M,H,q,F,G)$ and $S'(M,H,q,F)$ are provided in the Appendix. The parameter $\gamma/\mu^b h$ is the ratio of surface tension forces to the elastic forces and can be written as

$$\frac{\gamma}{\mu^b h} = \frac{\gamma}{\mu^a h^a}M(1-H) = G\,M(1-H), \quad \text{where} \quad G = \frac{\gamma}{\mu^a h^a}. \tag{23}$$

The bilayer can be visualized as a system of springs in series configuration with individual spring stiffnesses μ^a/h^a and μ^b/h^b. Thus, the parameter K_{eff}, the net effective elastic stiffness of the system, is given by the following expression:

$$K_{\text{eff}} = \frac{\frac{\mu^a}{h^a}\frac{\mu^b}{h^b}}{\frac{\mu^a}{h^a} + \frac{\mu^b}{h^b}}. \tag{24}$$

The nondimensional ratio $-Y/K_{\text{eff}}$ is hence a measure of the relative strength of the interaction stiffness at the top surface to the effective elastic stiffness offered by the bilayer, and its form is given as

$$-\frac{Y}{K_{\text{eff}}} = \frac{H(M-1)+1}{M}S''(M,H,q,F,G). \tag{25}$$

The purpose of the linear stability analysis is to find the critical value of the interaction stiffness ratio $(-Y_c/K_{\text{eff}})$ above which the interaction stiffness is strong enough to engender instabilities in the bilayer. Mathematically, this means obtaining the nontrivial values of the critical wave number q $(=q_c = k_c h)$ for which the characteristic equation Eq. (22) or (25) has a minimum for any particular set of values of H, M, F, and G.

The parameter H ranges from 0 to 1 while M lies in the range of 0 to ∞. A nondimensional parameter M_s $[=M/(1+M)]$ is introduced so that M can now be mapped from $0 < M < \infty$ to $0 < M_s < 1$. To uncover the critical wavelengths of instability $(\lambda_c = 2\pi/k_c)$ for an elastic bilayer, the contour plots of λ_c scaled with h are considered in the H-M_s plane for particular values of F and G. The lower limits of the parameter G (∼0.0) can be obtained when the surface tension is small (∼0.0). The parameter G can have high values (∼10) when the bottom layer has very small thickness (≪100 nm), high surface energy (∼100 mJ/m^2), and very small shear modulus values (∼0.1 MPa) such that the shear moduli of both soft elastic films are less than 10 MPa. Here we have considered three different values of G ($G \sim 0.0, 0.1, 10.0$) to study the effect of the parameter G on the instability length scales. Intermediate values of G between 0.1 and 10 and higher values of G are found to exhibit trends similar to that of $G = 10$ and hence are not presented in this paper. Three sample values of the amplitude ratio F are considered ($F = 0.1, 1.0, 5.0$) to understand the effect of the destabilizing forces arising due to interactions with the bottom substrate.

B. Asymptotic cases

The assembly of the bilayer is composed of a single elastic adhesive film on top of a wetting elastic film and the asymptotic limit of either of these two cases can be obtained from the characteristic equation [Eq. (22)].

Limit of a single elastic film in adhesive contact. The limit of a single elastic film in adhesive contact can be obtained from the characteristic equation Eq. (22) when $H \to 1.0$, $F = 0.0$, where the bilayer translates to the case of only the top film b being present in adhesive contact and yields the following single film equation:

$$\frac{-h^b Y}{\mu^b} = 2q\,\frac{1+\cosh(2q)+2q^2}{\sinh(2q)-2q}. \tag{26}$$

The right-hand side of Eq. (26) is a function of only the parameter q and hence the critical wavelength formed by minimizing this equation (∼$3h$) is universal in nature (independent of material properties of the film like the shear modulus or the surface tension and also independent of the nature of the force field present) as has been found in both experiments and simulations [21–42].

The elastic adhesive film can behave like a wetting film in adhesive contact if we consider the wetting limit $q \to 0$ [43–50] in Eq. (26):

$$\frac{-hY}{\mu} = \frac{3}{2}\left[\frac{[1+\cosh(2q)+2q^2]}{q^2}\right]. \tag{27}$$

It can be seen that Eq. (27) has functional variation in only q and exhibits a minimum at $\lambda_c/h = 2\pi/q_c = 5.23$ which may be short waved compared to the free wetting limit of h^2; however, it is much longer waved than the single elastic adhesive limit of $3h$.

III. RESULTS AND DISCUSSION

A. Variation in instability length scales

It would be interesting to study the predominant instability length scales that are exhibited by a general bilayer undergoing the squeezing mode of instability. The results of the linear stability analysis discuss these issues in the present section. The critical instability length scales with negligible surface tension effects ($G \sim 0$) and small amplitude ratios ($F = 0.1$) are shown in Fig. 2(a). Depending on the films' elastic stiffnesses (μ/h) and the length scales exhibited here, four distinct regions of instability can be identified in the parametric space of H-M_s:

Region I. $M_s \lesssim 0.5, H < 0.5$. Here, $h^a > h^b$ and $\mu^a < \mu^b$ and therefore $\mu^b/h^b > \mu^a/h^a$.

Region II. $M_s \lesssim 0.5, H > 0.5$. Here, $h^a < h^b$ and $\mu^a < \mu^b$. In this region elastic stiffnesses can be comparable or different depending on the values of H and M_s.

Region III. $M_s \gtrsim 0.5, H > 0.5$. This is the region where $h^a < h^b$ and $\mu^a > \mu^b$, and therefore $\mu^b/h^b < \mu^a/h^a$.

Region IV. $M_s \gtrsim 0.5, H < 0.5$. Here, $h^a > h^b$ and $\mu^a > \mu^b$. The elastic stiffnesses in this region can be comparable or different depending on the values of H and M_s (as in region II).

Throughout region I the instability length scales obtained are greater than the natural length scale of ∼$3h$ of single

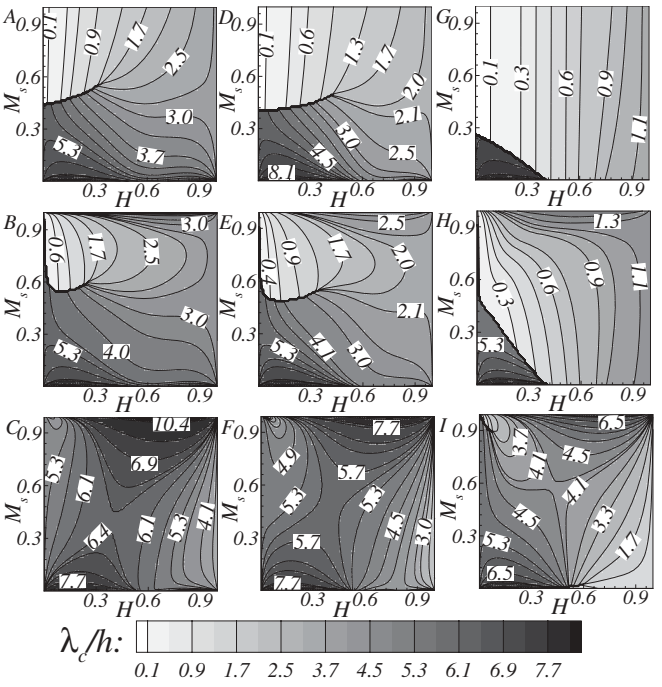

FIG. 2. Contour plots of the critical wavelength of instability λ_c/h in the H-M_s plane for various F and G values. (a) $F = 0.1, G \sim 0.0$; (b) $F = 0.1, G = 0.1$; (c) $F = 0.1, G = 10.0$; (d) $F = 1.0, G \sim 0.0$; (e) $F = 1.0, G = 0.1$; (f) $F = 1.0, G = 10.0$; (g) $F = 5.0$, $G \sim 0.0$; (h) $F = 5.0, G = 0.1$; (i) $F = 5.0, G = 10.0$.

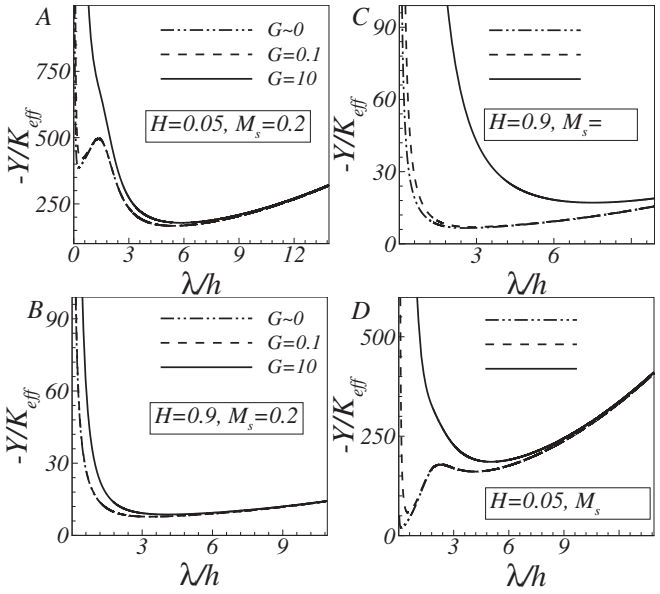

FIG. 3. Variation of interaction stiffness ratio $-Y_c/K_{\text{eff}}$ with λ/h in various regions of Figs. 2(a), 2(b), and 2(c) for $F = 0.1$. (a) Region I ($H = 0.05$, $M_s = 0.2$). For $G \sim 0$, the two minima (λ_c, $-Y_c/K_{\text{eff}}$) are (0.26h, 386.8) and (5.42h, 167.19); for $G = 0.1$, (0.41h, 418.58) and (5.43h, 167.312); and for $G = 10$, (5.85h, 178.54). (b) Region II ($H = 0.9$, $M_s = 0.2$). For $G \sim 0$, (λ_c, $-Y_c/K_{\text{eff}}$) are (3.33h, 7.78); for $G = 0.1$, (3.34h, 7.79); and for $G = 10$, (4.11h, 8.7). (c) Region III ($H = 0.9, M_s = 0.9$). For $G \sim 0$, ($\lambda_c, -Y_c/K_{\text{eff}}$) are (2.6$h$, 6.58); for $G = 0.1$, (2.88h, 7.01); and for $G = 10$, (7.51h, 17.12). (d) Region IV ($H = 0.05$, $M_s = 0.9$). For $G \sim 0$, (λ_c, $-Y_c/K_{\text{eff}}$) are (0.15h, 20.02) and (4.13h, 160.93); for $G = 0.1$, (0.52h, 58.16) and (4.15h, 161.23); and for $G = 10$, (5.03h, 185.65).

elastic adhesive film and can also be greater than the single wetting adhesive limit of 5.23h [as given by Eq. (27)]. The interaction stiffness landscape for this region presented in Fig. 3(a) suggests that two distinct minima are possible here—a short-wave minimum and a long-wave minimum, of which the global minimum corresponds to the longer wavelength. For example, for the parametric values of $G \sim 0$, $F = 0.1$, $H = 0.05$, and $M_s = 0.2$, the two minima are at $\lambda_c = 0.26h$ and $\lambda_c = 5.42h$ ($-Y_c/K_{\text{eff}} = 386.8$ and 167.19, respectively).

In the previous studies on interacting elastic thin films, it was found that the prevalent wavelength was dictated by the more compliant of the two films [24,35,57]. In this particular region, the top film is elastically much stiffer than the bottom film (i.e., $\mu^b/h^b > \mu^a/h^a$), rendering the bottom film to be the compliant film. This is illustrated by considering some of the values of $[(H, M_s); \frac{\mu^b/h^b}{\mu^a/h^a}]$ in this region, which are [(0.1, 0.1); 81], [(0.2, 0.1); 36], [(0.3, 0.1); 21], [(0.4, 0.1); 13.5], [(0.1, 0.2); 36], [(0.1, 0.3); 21], [(0.1, 0.4); 13.5], where the elastic stiffness of film b compared to that of film a, given by the third quantity in the parentheses, is always greater than 1. Hence, it can be understood that in this region the long-wave instability that prevails in the bilayer is mainly due to the influence of the predominantly compliant wetting bottom film.

This effect of the dominance of the compliant film can also be checked from the fact that for a particular value of H if M_s is decreased, the compliance of film a increases and this results in longer instability length scales. This can be observed from Fig. 2(a), where for $H = 0.1$ as M_s is decreased from 0.3 to 0.2, the λ_c increases from 4.97h to 5.41h. Similar observations can be made when M_s is kept constant and H is decreased, because in this direction also the compliance of film a increases. For example, in Fig. 2(a) for $M_s = 0.1$, as H is decreased from 0.3 to 0.2, λ_c increases from 5.49h to 6.05h.

As $H \to 0.0$, the bilayer system goes through a transition from an existent stiff top layer to a nonexistent top layer. This is reflected in the values of λ_c which approach a limiting value of 5.23h as $H \to 0.0$, which is the case of a single bottom wetting film in adhesive contact [see Eq. (27)]. For example in Fig. 2(a), for $M_s = 0.1$, when $H = 0.1$ the $\lambda_c = 6.26h$ and it decreases to the limit of 5.23h as $H \to 0.0$. Similar observations were made in elastic-metal bilayers consisting of a very thin, stiff metal layer cast on a very compliant elastic film, where it was found that if the top film thickness was very small, the length scales of instabilities formed were $\sim 3h$ and as the top layer thickness increased, the instabilities became very long waved [60]. The only difference from the current scenario is that in the elastic-metal bilayers, the bottom layer was not considered to be $\ll$100 nm, which would have triggered interactions with the substrate and engendered length scales of the order of 5.23h whenever the top layer was made to be very thin.

The inclusion of the surface energy parameter G in general is anticipated to have a stabilizing effect which will try to flatten out the film and consequently will increase the instability length scales. This very effect is visualized from Fig. 3(a) which shows the influence of G in the region I of Fig. 2(a). Fig. 3(a) shows that a slight increase in the value of surface energy G has negligible effect on the wavelengths but when G increases considerably, the nature of the interaction stiffness curve changes from having double minima at small G to having a single critical wavelength of instability, which is longer waved at large G (at $H = 0.05$, $M_s = 0.2$, $F = 0.1$, [G, λ_c]: [0,5.42h], [0.1,5.43h], [10,5.85h]). If we concentrate on region I, it can be seen that the contour plots of Fig. 2(a) (with $G \sim 0$) and Fig. 2(b) (with $G = 0.1$) are almost identical, with slight change in the values of the critical wavelength λ_c. Figure 2(c) (with $G = 10$), however, shows that the instabilities have become much longer waved comparatively.

When $H > 0.5$ and $M_s \lesssim 0.5$, i.e., in region II of Fig. 2(a), only one bifurcation mode is possible as can be observed from Fig. 3(b). For example, when $H = 0.9$ and $M_s = 0.2$, for very small values of G and F, the critical wavelength is short waved compared to those observed in region I. In this region, however, the shear modulus of the top film is greater than that of the bottom film throughout this domain. Thus the elastic stiffness, which is a ratio of the shear modulus of the film to the film thickness, of the top film decreases and its compliance becomes comparable to or greater than that of the bottom film as H increases (for example, for $M_s = 0.2$, $[H, \frac{\mu^b/h^b}{\mu^a/h^a}]$ vary as [0.6, 2.67], [0.8, 1], [0.95, 0.21]). From Fig. 2(a) it can be seen that as H increases (for any particular value of M_s), this effect is reflected in the formation of progressively shorter waved instabilities in this region [for example, if $M_s = 0.2$, $(H, \lambda_c) = (0.6, 3.52h)$ and $(0.95, 3.17h)$]. When the values of $F \to 0$, the wavelengths approach the natural length scales of 3h whenever $H \to 1$ [from Eq. (26)].

In this region too the stabilizing effect of increasing the surface tension parameter G is felt in the form of the increasing instability length scales as can be observed from Figs. 2(a), 2(b), and 2(c) and Fig. 3(b) [for $F = 0.1$, $H = 0.9$, and $M_s = 0.2$, $(G, \lambda_c) = (0.0, 3.33h)$, $(0.1, 3.34h)$, and $(10.0, 4.11h)$].

In region III of Fig. 2(a) there is only one dominant length scale of instability, as in region II, which is now short waved as depicted in Fig. 3(c). Here, the top film is highly compliant and its compliance increases as H or M_s increases and hence the adhesive nature of the more compliant top film engenders much smaller length scale instabilities when compared to regions I and II as evident from Fig. 2(a). In the absence of any significant surface tension and at very small values of the amplitude ratio, increasing H to the limiting value of 1 results in the critical instability length scales approaching the natural wavelength $3h$ of a single elastic adhesive film. An increase in M_s in this region by fixing the value of H results in a very compliant top film (compared to that of the bottom film), which now becomes the dictating film, and is seen to engender progressively shorter length scales, even less than the single elastic adhesive limit of $3h$. For example for $F = 0.1$, $G \sim 0$, and $H = 0.6$ of Fig. 2(a), the values of (M_s, λ_c) are $(0.6, 2.39h)$ and $(0.9, 1.82h)$.

As the surface tension parameter G is increased, the resulting instabilities are long waved as expected and the effect is very dramatic for high values of surface tension, as can be seen from Figs. 2(a), 2(b), and 2(c) and Fig. 3(c). For example, for $H = 0.9$, $M_s = 0.9$, and $F = 0.1$, the values of $[G, \lambda_c]$ are $[0, 2.60h]$, $[0.1, 2.88h]$, and $[10, 7.51h]$. The surface tension effect comes through the parameter $G\,M(1 - H)$ as shown in Eq. (23), which translates to the dimensional form $\gamma/\mu^b h$. As M_s increases, the shear modulus of the top film (μ^b) decreases and the value of $\gamma/\mu^b h$ escalates. It can thus be seen that the long-wave behavior brought in by G is accentuated as one moves to higher values of M_s in region III.

In region IV of Fig. 2(a), when the surface tension is negligible, two wavelengths of instability are possible of which the shorter instability wavelength prevails as can be seen from Fig. 3(d). The formation of shorter instabilities in region IV can be attributed to the fact that the top film is less stiffer in region IV when compared to region I ($\mu^b/h^b = 36\mu^a/h^a$ when $M_s = 0.2$, $H = 0.1$ in region I and $\mu^b/h^b = 0.47\mu^a/h^a$ when $M_s = 0.95$, $H = 0.1$ in region IV) and the short-wave instabilities as dictated by the more compliant top film prevail. However, as $H \to 0$ the top film b is stiffer than the bottom film a in both regions I and IV, and the instability wavelengths attain a limiting value of $5.23h$ (limit of the single wetting elastic adhesive film). This transition happens suddenly as $H \to 0$ and cannot be seen distinctly in Fig. 2(a). An earlier work on elastic bilayers with "bending" modes of instability (without surface tension effects) had also theoretically predicted that at high values of M_s, with decrease in H there are two instability wavelengths possible and the smaller instability wavelength is predominant [57]. Length scales as small as ~0.5h were also possible at sufficiently large values of M_s and small values of H. However, a qualitative and quantitative difference exists in both the results as both the films considered in the earlier study were of finite thickness and hence the films always deformed in a *bending* mode unlike the present work where the films deform in a *squeezing* mode.

Whenever the surface tension increases to high values, there is a shift from double minima in the interaction stiffness curves to a single minimum which is longer waved as evident from Fig. 3(d). The effect of surface tension is particularly amplified in region IV where the percentage change in λ_c is the highest. This is because H is smallest and M_s is largest in this region and it is now understood that the surface energy effect is $\propto G M_s(1 - H)/(1 - M_s)$ and this value is highest in region IV. Hence, in region IV as the surface energy contribution G increases, there is a shift from the shorter wavelengths in Fig. 2(a) to longer wavelengths in Fig. 2(c) (for example, for $H = 0.05$, $M_s = 0.9$, and $F = 0.1$, the values of $[G, \lambda_c]$ are $[0,0.15h]$, $[0.1,0.52h]$, and $[10,5.03h]$).

The amplitude ratio F extends a very pronounced effect on the critical instability length scales in region I as we move from Fig. 2(a) where F is very small ($F = 0.1$ and $G \sim 0.0$) to Fig. 2(g) where $F = 5.0$ and $G \sim 0.0$. Here it is observed that as F increases, in a small region where $H \to 0$ and $M_s \to 0$, the instabilities still remain long waved as dictated by the more compliant bottom film as seen earlier for smaller values of F. However, for higher values of H and M_s in this region it can be observed that short-wave instabilities are favored, due to the top film overpowering the influence exerted by the more compliant bottom film. In the other regions II, III, and IV, where the top film already has a dominating influence, an increase in the value of F requires an increase in the destabilizing influence (as can be verified later from $-Y_c/K_{\text{eff}}$ values produced) and is seen to result in further reduction in the length scales [refer to Figs. 2(a), 2(d), and 2(g)].

For other values of $G > 0$, it is seen from Figs. 2(e), 2(f), 2(h), and 2(i) that F has a similar effect in bringing down the instability length scales. The exact amplitude ratio F that the film-film interface exhibits is not a controllable parameter and can be understood completely only if a nonlinear study is carried out, which is beyond the scope of the present work. However, a suggestive study is done by varying F to get an insight into the instability length scales that may form due to very strong interactions from the substrate.

B. Variation in critical interaction penalty

The effective elastic stiffness (K_{eff}) that the bilayer offers in resistance to the destabilizing interactions is very high in region I and it decreases as H or M_s increases and reaches lowest values in the limit $H \to 1$ and $M_s \to 1$. For example, (H, M_s, K_{eff}) take the values of $(0.11, 0.25, 0.96\mu^a/h^a)$, $(0.11, 0.9, 0.47\mu^a/h^a)$, $(0.9, 0.25, 0.25\mu^a/h^a)$, and $(0.9, 0.9, 0.01\mu^a/h^a)$ in regions I, IV, II, and III, respectively. The factor $-Y_c/K_{\text{eff}}$ is a measure of the critical force required at the top interface to destabilize the bilayer by overcoming this effective elastic stiffness and is shown in Fig. 4. When the bilayer has negligible surface tension and the amplitude ratio is also small, the effect of H and M_s on the interaction stiffness ratio $(-Y_c/K_{\text{eff}})$ present at the bilayer-air interface is shown in Fig. 4(a). It is seen that $-Y_c/K_{\text{eff}}$ is highest in region I, followed by regions IV, II, and III. The true critical interaction stiffness required for destabilization is much higher in region I due to the high K_{eff} values brought in by a very thin and stiff top layer in this region. As we move from region I to region IV by increasing M_s for any particular value of H or to region II by

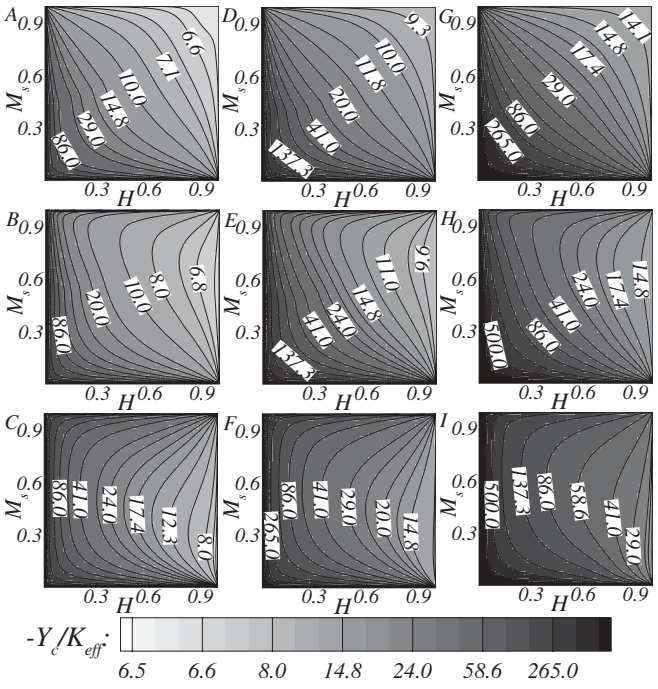

FIG. 4. Contour plots of the critical interaction penalty ratio $-Y_c/K_{\text{eff}}$ in the H-M_s plane for various F and G values. (a) $F = 0.1, G \sim 0.0$; (b) $F = 0.1, G = 0.1$; (c) $F = 0.1, G = 10.0$; (d) $F = 1.0, G \sim 0.0$; (e) $F = 1.0, G = 0.1$; (f) $F = 1.0, G = 10.0$; (g) $F = 5.0, G \sim 0.0$; (h) $F = 5.0, G = 0.1$; (i) $F = 5.0, G = 10.0$.

increasing H for any particular value of M_s, the compliance of film b increases and this results in smaller interaction penalty requirement compared to the region I. For example, for the parameter values of $F = 0.1$, $G \sim 0$, the $(H, M_s; -Y_c)$ values are $(0.11, 0.25; 72\mu^a/h^a)$, $(0.11, 0.9; 5.78\mu^a/h^a)$, and $(0.9, 0.25; 1.85\mu^a/h^a)$ in regions I, IV, and II, respectively.

Within region III, both the critical interaction stiffness ratios depicted and the actual interaction penalties required are much less as the compliance of the top film is highest in this region and it undergoes deformation very easily [for example, for $F = 0.1$, $G \sim 0$ in Fig. 4(a), the values of $(H, M_s; -Y_c)$ in region III are $(0.9, 0.9; 0.083\mu^a/h^a)$].

Since the surface energy has a stabilizing effect in case of adhesive films, it is reflected even in the net interaction stiffness ratio plots Figs. 4(b) and 4(c); i.e., as G increases, much higher interaction penalty is required for the bilayer to overcome these additional stabilizing effects and lose its planarity. For example, for $F = 0.1$ and the same set of parameters of H, M_s considered in the beginning of this section, the interaction penalty $(-Y_c)$ values for $G = (0.1; 10)$ are $(72.12\mu^a/h^a;\ 81.91\mu^a/h^a)$, $(1.85\mu^a/h^a;\ 2.14\mu^a/h^a)$, $(0.09\mu^a/h^a;\ 0.21\mu^a/h^a)$, and $(12.85\mu^a/h^a;\ 47.84\mu^a/h^a)$ in regions I, II, III, and IV, respectively.

When F increases, there is an increase in amplitude of deformation at the lower surface of the top film, brought about by an increase in interactions arising due to the bottom substrate. This engenders a high critical interaction penalty requirement in all the regions to overcome these additional interactions and cause deformation of the top interface of the upper film as evident from Figs. 4(a), 4(d), and 4(g).

An increase in surface tension parameter G or a requirement of high F results in high interaction penalties as discussed above, and when both F and G are very high simultaneously, the penalties required escalate as can be observed from Figs. 4(e), 4(f), 4(h), and 4(i).

C. Variation in interfacial displacement jump

The no-slip boundary condition of Eq. (12) at the film-film interface only ensures continuity of the transverse displacements and the interface imperfection factor β_t in Eq. (14) is infinite under such conditions. There is nevertheless a possibility of delamination of the interfaces which would result in a positive, nonzero finite value of the interface imperfection factor β_n as mentioned in the previous sections. From Fig. 5 it is observed that the film-film interface shows normal displacement jumps, leading to delamination of the interface. The interface delamination magnitude is considered to be $\Delta u_2 = u_2^a(x_1, -h^b) - u_2^b(x_1, -h^b)$ and it is scaled with $\alpha \cos(k_c x_1)$ (the equilibrium displacement profile of the bilayer-air interface). The displacement jumps shown here correspond to the critical conditions of instability presented in Figs. 2 and 4. From Fig. 5(a) for $F = 0.1$ and $G \sim 0$, it is evident that in region I large displacement jumps are present and this can be understood considering that in this region the top film is much thinner and of much higher stiffness compared to the bottom film. Thus, the top film cannot deform coherently with the bottom film, though it is under the influence of strong interaction forces from the contactor. The only possible

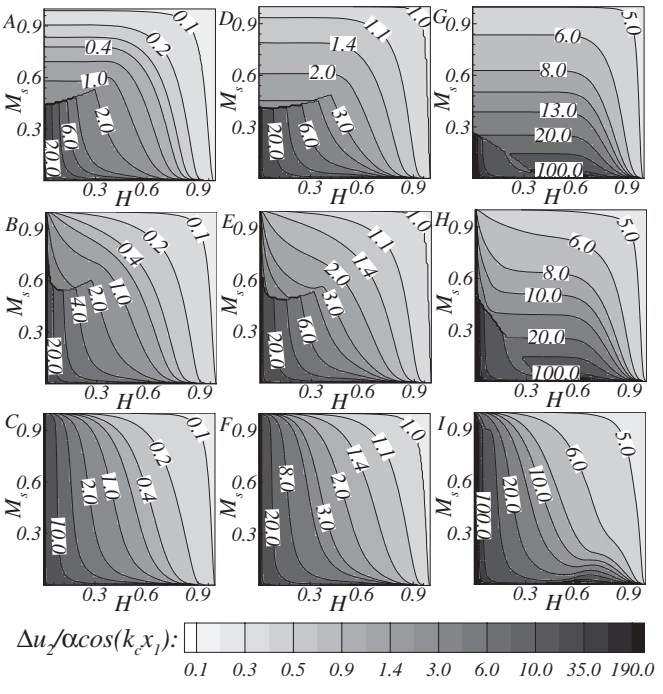

FIG. 5. Contour plots of the jumps in the normal displacements at the film-film interface $\Delta u_2/\alpha \cos(k_c x_1)$ in the H-M_s plane for various F and G values. (a) $F = 0.1, G \sim 0.0$; (b) $F = 0.1, G = 0.1$; (c) $F = 0.1, G = 10.0$; (d) $F = 1.0, G \sim 0.0$; (e) $F = 1.0, G = 0.1$; (f) $F = 1.0, G = 10.0$; (g) $F = 5.0, G \sim 0.0$; (h) $F = 5.0, G = 0.1$; (i) $F = 5.0, G = 10.0$.

mode of relieving these excess stresses would therefore be to delaminate, as is evident from the excessive jump in normal displacement at the film-film interface in region I. The magnitude of the jumps increase with an increase in the stiffness of the top film, i.e., as either H or M_s decreases. For example, for $F = 0.1$, $G \sim 0$, the values of $(H, M_s; \Delta u_2/\alpha \cos(k_c x_1))$ in Fig. 5(a) are (0.4, 0.4; 1.497), (0.1, 0.4; 8.805), and (0.4, 0.1; 2.822). This is similar to the observations made in a previous work on dissimilar elastic films undergoing in-plane compressive stresses, where it was seen that as the compliance of the underlying layer increased the films delaminated more easily [68].

The top film is more compliant in regions II, III, and IV than in region I and this results in relatively smaller displacement jumps as can be seen from Fig. 5(a). Moreover, as one moves to higher values of H and M_s, the parameter $\Delta u_2/\alpha \cos(k_c x_1)$ decreases and reaches its lowest limiting value of F when $H \to 1$ and $M_s \to 1$. This suggests that the top surface of the bottom film has a zero displacement in this limit which is because the bottom layer is very stiff and behaves as a part of the rigid substrate, making it difficult to undergo any deformation. The displacement profile of the top film at the film-film interface is $-F\alpha \cos(k_c x_1)$ whereas that of the bottom film is found to be $(\Delta u_2 - F)\alpha \cos(k_c x_1)$. It is evident from Fig. 5 that Δu_2 is always positive and greater than F and thus, it can be concluded that both the films are always completely out of phase at the film-film interface, exhibiting varicose instabilities/blister formation. This can also be inferred from the values of β_n which are very small ($0.01 < \beta_n < 10$) in region I suggesting that there is a significant jump in normal displacement at the film-film interface in region I. As either H or M_s increases, the values of β_n increase, reaching magnitudes of the order of 10^6 when $M_s \to 1$ (i.e., when the top film is very compliant), suggesting very less delamination at the film-film interface in such regions.

As the surface tension increases, it tries to stabilize the bilayer and results in a decrease in the normal displacement jumps, in general, as can be observed from Figs. 5(a), 5(b), and 5(c), which also results in higher values of the interface imperfection factor. However, in region IV an increase in G helps the bilayer to achieve long-wave instabilities and the bilayer now behaves the same way as in region I, resulting in the same degree of delamination (as that in region I).

For any particular value of the surface tension parameter G, an increase in F would mean higher amplitude of deformations at the film-film interface, which generally requires stronger interactions from the substrate and if the bottom layer is very compliant as in region I, stronger interactions would deform it with higher amplitudes. Since the film-film interface deforms in varicose mode, such higher amplitude instabilities in both the films at the film-film interface lead to a higher degree of delamination [for example, refer to Figs. 5(a), 5(d), and 5(g)] and engenders very small values of the interface imperfection factor (β_n). When the bottom layer becomes very stiff (as in region III), it is difficult for it to deform even when the interactions from the substrate are very strong and the delamination magnitude is limited to the value of F in the limit $H \to 1$, $M_s \to 1$.

IV. CONCLUSIONS

Previous studies have shown that elastic bilayers in contact proximity with an external contactor do display patterns with miniature length scales $<3h$ (single adhesive elastic film limit). In the experiments the focus was on determining the instability length scales at the surface [58,59] and it is difficult to conclude from these whether the two interfaces of the bilayer deform in-phase (*bending mode*) or out-of-phase (*squeezing mode*). The corresponding theoretical work, however, has suggested that it is energetically unfavorable for the film-film interface to deform out-of-phase [57]. In this paper it is shown that if the bilayer is comprised of a bottom layer which is very thin ($\ll$100 nm) such that the interactions of the film-film interface with the substrate become important, the *squeezing mode* of instability is feasible and a myriad of instability length scales ranging from $0.1h$ to $10h$, which are much lower than $3h$, the single elastic adhesive limit, and much higher than $5.23h$, the single wetting adhesive limit, are formed.

(1) In region I, where the elastic stiffness (shear modulus to thickness ratio) of the top film is very high, the instability length scales are largely governed by the more compliant bottom film and are very long waved ($\sim 10h$). From region I if one moves either to region II by increasing the thickness of the top layer or to region IV by decreasing the shear modulus of the top layer, the elastic stiffness of the top film decreases to become comparable to or less than that of the bottom layer, and there is a shift in the wavelengths towards shorter length scales. The effect is more dramatic in region IV where the length scales are the lowest, becoming as small as $0.1h$ at very low values of the surface tension, whereas the lowest length scales achieved in region II are restricted to the single elastic adhesive limit of $3h$. The stiffness of the top film is lowest in region III and as $H \to 1$, the bottom layer becomes nonexistent and the instabilities formed are of length scales $\sim 3h$. Whenever the top film is much thicker and has very small shear modulus compared to the bottom film, as in region III, the interaction penalty requirements are the lowest. In the regions where the top film is very stiff in comparison to the bottom film, the interaction penalty requirement from the contactor to deform the top film increases tremendously and thus is found to be highest in region I.

(2) It is observed that the interface becomes *imperfect* and there are jumps in the normal displacements at the film-film interface, and the deformations that occur at the film-film interface are varicose in nature and may result in delamination/blistering. The degree of delamination increases as the compliance of the top film decreases and the delamination magnitudes are highest in region I. This confirms earlier findings of dissimilar elastic films undergoing in-plane compressive stresses that the degree of delamination increases as the stiffness of the top film increases [70]. When the bottom film is excessively stiff compared to that of the top film, it does not undergo any deformation and the magnitude of the delamination is the lowest (reaching a limiting value of F). This degree of delamination is also quantified by the interface imperfection constant β_n which is a property of the interface given by the values of H, M_s, G, and F and ranges from 0.01 in region I where the delamination magnitudes are the highest to 10^6 in region IV where the delamination magnitudes are the lowest.

(3) Increasing the surface tension increases the stability of the bilayer and results in longer length scales of instability throughout the parametric space considered. In the limit of a very thin top layer, it makes the bilayer behave the same for every shear modulus ratio as is evident from the length scales and the displacement jumps obtained in these regions. Also, any increase in surface tension makes the film difficult to deform against these stabilizing effects, and thus the interaction penalty required to deform the bilayer increases significantly when the surface tension increases to very high values. The stabilizing effect of the surface tension, in general, tries to suppress the degree of delamination of the interfaces and the value of the interface imperfection factor β_n escalates.

(4) The deformations at the bottom surface of the top film, characterized by the parameter F, are resultant of the interactions present at the bottom substrate, and stronger interactions would result in higher values of F. It is seen that as the value of F increases, the interaction penalty required to deform the top surface of the bilayer increases since it has to surpass the strong interactions from the bottom substrate as well and results in much shorter waved instabilities. Since the film-film interface deforms in varicose mode, high-amplitude instabilities at the film-film interface are found to result in a higher degree of delamination characterized by the smaller values of the interface imperfection factor β_n.

The smallest wavelengths obtained by this elastic bilayer route through squeezing instabilities are $0.1h$, which is smaller than the smallest length scales reported to date, i.e., $3h$ that was reported with single elastic film [21–42], $0.5h$ that was reported with an elastic bilayer undergoing bending modes of instability at the two interfaces [56,57], and $0.3h$ that was obtained with a single elastic film cast on patterned substrates [55]. From a fabrication point of view, the smallest patterns can be obtained when the surface energies are very low and the top film is considered to be much thinner and of very small shear modulus than the bottom film (corresponding to the material properties of region IV as discussed in this paper). For other thickness and shear moduli ratios, the length scales can be miniaturized if very strong interactions are present between the bottom film and the substrate, but this has the disadvantage of increasing the delamination magnitude at the film-film interface.

ACKNOWLEDGMENT

The authors acknowledge the Department of Science and Technology, New Delhi, for supporting this project.

APPENIDX

$$
\begin{aligned}
S'(M,H,q,F) = \{&(H-1)Hq[8Fe^{(5H+2)q}\{M[2H^3q^3+2H^2(1-2q)q^2+H(2q^2-4q+1)q+2q^2+1]\\
&-2(H-1)q[H^2q^2-H(q-1)q+1]\}-8Fe^{(3H+2)q}\{M[2H^3q^3-2H^2(2q+1)q^2\\
&+H(2q^2+4q+1)q-2q^2-1]-2(H-1)q[H^2q^2-H(q+1)q+1]\}\\
&-4F(M-1)e^{(H+4)q}(Hq-1)-4F(M+1)e^{5Hq}(Hq-1)+4F(M-1)e^{7Hq}(Hq+1)\\
&+4F(M+1)e^{(3H+4)q}(Hq+1)+2e^{2(H+2)q}+\{M[G(H-1)q+4H^2q^2+2]\\
&+2G(H-1)HM^2q^2+4Hq\}+2e^{6Hq}\{M[G(q-Hq)+4H^2q^2+2]\\
&+2G(H-1)HM^2q^2-4Hq\}+8e^{4Hq+2q}(M\{-q^2[G(H-1)^2-4H^2+4H-2]\\
&-2(H-1)^2Hq^4[G(H-1)-2H]+1\}+G(H-1)HM^2q^2[2(H-1)^2q^2+1]q)[G(H-1)Mq-2]\\
&-4(H-1)Hq^2(H^2q^2-Hq^2+1)]-2e^{6Hq+2q}(M[2(H-1)^2q^2+1]-2(H-1)\\
&+2e^{2(H+1)q}\{M[2(H-1)^2q^2+1]+2(H-1)q\}[G(H-1)Mq+2]-(M-1)e^{8Hq}[G(H-1)Mq-2]\\
&-(M+1)e^{4(H+1)q}[G(H-1)Mq-2]+(M-1)e^{4q}[G(H-1)Mq+2]\\
&+(M+1)e^{4Hq}[G(H-1)Mq+2]\}/[[H(M-1)+1](8qe^{4Hq+2q}[2H^3(M-1)q^2-4H^2(M-1)q^2\\
&+H(M-1)(2q^2+1)+1]-2e^{6Hq+2q}\{M[2(H-1)^2q^2+1]-2(H-1)q\}\\
&+2e^{2(H+1)q}\{M[2(H-1)^2q^2+1]+2(H-1)q\}-(M-1)e^{8Hq}+(M+1)e^{4Hq}-(M+1)e^{4(H+1)q}\\
&+e^{6Hq}(4HMq-2)+e^{2(H+2)q}(4HMq+2)+(M-1)e^{4q})]
\end{aligned}
\tag{A1}
$$

$$
S''(M,H,kh,F,G) = S'(M,H,q,F)+Gq^2M(1-H) \tag{A2}
$$

[1] M. Watanabe, H. Shirai, and T. Hirai, J. Appl. Phys. **92**, 4631 (2002).

[2] S. P. Lacour, S. Wagner, Z. Huang, and Z. Suo, Appl. Phys. Lett. **82**, 2404 (2003).

[3] Z. Hu, M. Tian, B. Nysten, and A. M. Jonas, Nat. Mater. **8**, 62 (2009).

[4] F. Zhang, T. Nyberg, and O. Inganäs, Nano Lett. **2**, 1373 (2002).

[5] J. R. Lawrence, P. Andrew, W. L. Barnes, M. Buck, and G. A. Turnbull, Appl. Phys. Lett. **81**, 1955 (2002).

[6] T. W. Lee, J. Zaumsiel, S. H. Kim, and J. W. P. Hsu, Adv. Mater. **16**, 2040 (2004).

[7] P. Muralt, J. Micromech. Microeng. **10**, 136 (2000).
[8] A. Kros, R. J. M. Nolte, and N. A. J. M. Sommerdijk, Adv. Mater. **14**, 1779 (2002).
[9] A. J. Crosby and K. R. Shull, J. Polym. Sci., Part B: Polym. Phys. **37**, 3455 (1999).
[10] Y. Y. Lin, C. Y. Hui, and H. D. Conway, J. Polym. Sci., Part B: Polym. Phys. **38**, 2769 (2000).
[11] A. J. Crosby, K. R. Shull, H. Lakrout, and C. Creton, J. Appl. Phys. **88**, 2956 (2000).
[12] T. Yamaguchi, H. Morita, and M. Doi, Eur. Phys. J. E **20**, 7 (2006).
[13] A. Khademhosseini, K. Y. Suh, S. Jon, G. Eng, J. Yeh, G. J. Chen, and R. Langer, Anal. Chem. **76**, 3675 (2004).
[14] W. Tan and T. A. Desai, Biomaterials **25**, 1355 (2004).
[15] T. M. Squires and S. R. Quake, Rev. Mod. Phys. **77**, 977 (2005).
[16] H. Miyajima and M. Mehregany, J. Microelectromech. Syst. **4**, 220 (1995).
[17] A. Singh, J. Jayaram, M. Madou, and S. Akbar, J. Electrochem. Soc. **149**, 78 (2002).
[18] X. Wang, J. Engel, and C. Liu, J. Micromech. Microeng. **13**, 628 (2003).
[19] Y. Fu, S. Du, W. Huang, S. Zhang, and M. Hu, Sensors and Actuators A **112**, 395 (2004).
[20] B. Y. Yoo, S. C. Hernandez, D.-Y. Park, and N. V. Myung, Electrochim. Acta **51**, 6346 (2006).
[21] W. Mönch and S. Herminghaus, Europhys. Lett. **53**, 525 (2001).
[22] V. Shenoy and A. Sharma, Phys. Rev. Lett. **86**, 119 (2001).
[23] V. Shenoy and A. Sharma, J. Mech. Phys. Solids **50**, 1155 (2002).
[24] J. Sarkar, V. Shenoy, and A. Sharma, Phys. Rev. E **67**, 031607 (2003).
[25] V. Shenoy and A. Sharma, J. Appl. Phys. **94**, 6376 (2003).
[26] J. Sarkar, V. Shenoy, and A. Sharma, Phys. Rev. Lett. **93**, 018302 (2004).
[27] J. Sarkar, A. Sharma, and V. Shenoy, Langmuir **21**, 1457 (2005).
[28] J. Sarkar, A. Sharma, and V. Shenoy, J. Adhes. **81**, 271 (2005).
[29] N. Arun, A. Sharma, V. Shenoy, and K. S. Narayan, Adv. Mater. **18**, 660 (2006).
[30] E. Fried and R. E. Todres, J. Elast. **80**, 97 (2005).
[31] S. Q. Huang, Q. Y. Li, X. Q. Feng, and S. W. Yu, Mech. Mater. **38**, 88 (2006).
[32] M. Gonuguntla, A. Sharma, and S. A. Subramanian, Macromolecules **39**, 3365 (2006).
[33] M. Gonuguntla, A. Sharma, R. Mukherjee, and S. A. Subramanian, Langmuir **22**, 7066 (2006).
[34] M. Gonuguntla, A. Sharma, J. Sarkar, S. A. Subramanian, M. Ghosh, and V. Shenoy, Phys. Rev. Lett. **97**, 018303 (2006).
[35] J. Y. Chung, K. H. Kim, M. K. Chaudhury, J. Sarkar, and A. Sharma, Eur. Phys. J. E **20**, 47 (2006).
[36] N. Arun, J. Sarkar, A. Sharma, V. Shenoy, and K. S. Narayan, J. Adhes. **83**, 513 (2007).
[37] S. Q. Huang, B. Li, and X. Q. Feng, J. Appl. Phys. **103**, 083501 (2008).
[38] J. Sarkar, A. Sharma, and V. B. Shenoy, Phys. Rev. E **77**, 031604 (2008).
[39] N. Arun, A. Sharma, P. S. G. Pattader, I. Banerjee, H. M. Dixit, and K. S. Narayan, Phys. Rev. Lett. **102**, 254502 (2009).
[40] X. H. Pan, S. Q. Huang, S. W. Yu, and X. Q. Feng, J. Phys. D **42**, 055302 (2009).
[41] J. Sarkar and A. Sharma, Langmuir **26**, 8464 (2010).
[42] Y.-C. Chen, E. Fried, and D. A. Tortorelli, J. Mech. Phys. Solids **60**, 904 (2012).
[43] G. Reiter, Phys. Rev. Lett. **68**, 75 (1992).
[44] A. Sharma and R. Khanna, Phys. Rev. Lett. **81**, 3463 (1998).
[45] G. Reiter, R. Khanna, and A. Sharma, Phys. Rev. Lett. **85**, 1432 (2000).
[46] R. Seemann, S. Herminghaus, and K. Jacobs, Phys. Rev. Lett. **86**, 5534 (2001).
[47] K. Kargupta and A. Sharma, J. Colloid Interface Sci. **245**, 99 (2002).
[48] R. Verma, A. Sharma, K. Kargupta, and J. Bhaumik, Langmuir **21**, 3710 (2005).
[49] J. C. T. Kao, A. A. Golovin, and S. H. Davis, J. Colloid Interface Sci. **303**, 532 (2006).
[50] R. Verma, A. Sharma, I. Banerjee, and K. Kargupta, J. Colloid Interface Sci. **296**, 220 (2006).
[51] R. Mukherjee, D. Bandyopadhyay, and A. Sharma, Soft Matter **4**, 2086 (2008).
[52] X. Tian and B. Bhushan, J. Phys. D **29**, 163 (1996).
[53] B. Bhushan and C. Dandavate, J. Appl. Phys. **87**, 1201 (2000).
[54] T. Vilmin, E. Raphael, P. Damman, S. Sclavons, S. Gabriele, M. Hamieh, and G. Reiter, Europhys. Lett. **73**, 906 (2006).
[55] J. Sarkar, H. Annepu, and A. Sharma, J. Adhes. **87**, 214 (2011).
[56] J. Yoon, C. Q. Ru, and A. Mioduchowski, J. Appl. Phys. **98**, 113503 (2005).
[57] G. Tomar, A. Sharma, V. Shenoy, and G. Biswas, Phys. Rev. E **76**, 011607 (2007).
[58] R. Mukherjee, R. Pangule, A. Sharma, and G. Tomar, Adv. Funct. Mater. **17**, 2356 (2007).
[59] R. Mukherjee and A. Sharma, ACS Appl. Mater. Interfaces **4**, 355 (2012).
[60] R. C. Pangule, I. Banerjee, and A. Sharma, J. Chem. Phys. **128**, 234708 (2008).
[61] D. Bandyopadhyay and A. Sharma, J. Colloid Interface Sci. **311**, 595 (2007).
[62] D. Bandyopadhyay, R. Gulabani, and A. Sharma, Ind. Eng. Chem. Res. **44**, 1259 (2005).
[63] D. Bandyopadhyay and A. Sharma, J. Chem. Phys. **125**, 054711 (2006).
[64] D. Bandyopadhyay, A. Sharma, and V. Shankar, J. Chem. Phys. **128**, 154909 (2008).
[65] A. A. Volinsky, N. R. Moody, and W. W. Gerberich, Acta Mater. **50**, 441 (2002).
[66] P. Peyla, Phys. Rev. E **62**, R1501 (2000).
[67] M. George, C. Coupeau, J. Colin, F. Cleymand, and J. Grilhé, Philos. Mag. A **82**, 633 (2002).
[68] H.-H. Yu and J. W. Hutchinson, Int. J. Fract. **113**, 39 (2002).
[69] H. Mei, R. Huang, J. Y. Chung, C. M. Stafford and H.-H. Yu, Appl. Phys. Lett. **90**, 151902 (2007).
[70] D. Vella, J. Bico, A. Boudaoud, B. Roman, and P. M. Reis, Proc. Natl. Acad. Sci. USA **106**, 10901 (2009).
[71] H. Mei, C. M. Landis, and R. Huang, Mech. Mater. **43**, 627 (2011).
[72] C. J. van Oss, M. K. Chaudhury, and R. J. Good, Chem. Rev. **88**, 927 (1988).
[73] Z. Hashin, Mech. Mater. **8**, 333 (1990).
[74] Z. Hashin, J. Mech. Phys. Solids **39**, 745 (1991).
[75] J. Qu, Mech. Mater. **14**, 269 (1993).
[76] Y. A. Antipov, O. Avila-Pozos, S. T. Kolaczkowski, and A. B. Movchan, Int. J. Solids Struct. **38**, 6665 (2001).

[77] Y. Benveniste and T. Miloh, Mech. Mater. **33**, 309 (2001).
[78] Z. Hashin, J. Mech. Phys. Solids **50**, 2509 (2002).
[79] S. Udea, S. Biwa, K. Watanabe, R. Heuer, and C. Pecorari, Int. J. Eng. Sci. **44**, 874 (2006).
[80] X.-C. Zhong, X.-F. Li, and K. Y. Lee, Int. J. Solids Struct. **46**, 1456 (2009).
[81] W. Q. Chen, Y. Y. Zhou, C. F. Lü, and H. J. Ding, Eur. J. Mech. A **28**, 720 (2009).
[82] X.-C. Zhong and K.-S. Zhang, Appl. Math. Mech. **33**, 357 (2012).
[83] H. Y. Yu, Y. N. Wei, and F. P. Chiang, Int. J. Eng. Sci. **40**, 1647 (2002).